

Orthogonally Constrained CASSCF Framework: Newton-Raphson Orbital Optimization and Nuclear Gradients

Loris Delafosse,¹ Vincent Robert,¹ and Saad Yalouz¹

Laboratoire de Chimie Quantique, Institut de Chimie, CNRS/Université de Strasbourg, 4 rue Blaise Pascal, 67000 Strasbourg, France

(*Electronic mail: saad.yalouz@cnrs.fr)

(Dated: January 28, 2026)

In a recent work¹, we introduced the foundations of an orthogonally constrained complete active space self-consistent field (OC-CASSCF) framework that produces state-specific molecular orbitals for mutually orthogonal multiconfigurational electronic states. In the present study, we extend this approach by incorporating a Newton-Raphson orbital-optimization scheme, for which we derive analytical expressions of the orbital gradient and Hessian. Furthermore, we outline a practical route toward the evaluation of analytical nuclear gradients, enabling geometry optimizations within the OC-CASSCF formalism. Benchmark calculations on the three lowest singlet states of LiH and H₂O molecules demonstrate a systematic improvement as compared to conventional state-averaged CASSCF, even when using modestly sized active spaces.

INTRODUCTION

A central challenge in electronic structure theory concerns the development of computational methods that can accurately describe both ground- and excited-state properties. This question naturally arises from the increasing need to model complex molecular processes in which strong electronic correlations simultaneously affect multiple states. Illustrative examples include photochemical reactions and their applications in therapy^{2,3}, molecular magnetism^{4–8}, and electron transfer processes^{9,10}.

In wavefunction-based methodologies, a broad range of approaches has been proposed to address this challenge. At the single-particle level, extended mean-field methods^{11–14} have been developed to optimize molecular orbitals (MOs) for specific excited states. Beyond mean-field approximations, numerous multiconfigurational methods have been introduced to capture electronic correlation effects. These include configuration-interaction (CI) expansions combined with Monte-Carlo techniques^{15–19}, density-matrix renormalization group methods^{20–23}, coupled-cluster approaches^{24–26}, and even strategies designed for quantum computers^{27–31}. Apart from Full-CI (FCI) expansions, the accuracy of truncated multi-configurational methods depends on the choice of the MO basis set. Optimizing orbitals for specific states therefore emerges as a crucial step.

Building on this principle, the Complete-Active-Space Self-Consistent Field (CASSCF) framework^{32,33} remains a reference. By combining a reduced CAS-CI expansion with orbital optimization, the CASSCF method provides a balanced and variationally motivated treatment of static correlation effects. In its state-averaged formulation (SA-CASSCF), a common set of MOs is optimized over an ensemble of states, yielding mutually orthogonal many-electron wavefunctions. While “state averaging” offers a convenient mathematical trick for multi-state calculations, the use of shared orbitals suppresses state-specific orbital relaxation, making excitation energies and properties sensitive to the number and nature of states included in the ensemble. By contrast, the state-

specific formulation (SS-CASSCF) allows full orbital relaxation for a targeted state. However, because it does not satisfy a variational principle for excited states, SS-CASSCF is known to be prone to root flipping and variational collapse toward lower-lying states. Despite this limitation, note that recent studies have shown that SS-CASSCF can sometimes achieve improved accuracy with smaller CAS^{36,37} compared to state-averaged approaches.

The variational collapse inherent to SS-CASSCF can be seen as a consequence of the absence of explicit orthogonality constraints between independently optimized states. To address this issue, we have recently laid the foundations of an orthogonally constrained (OC) version of CASSCF (OC-CASSCF)¹, in which excited states are optimized to remain orthogonal to previously computed states (note that similar strategies have also been considered in other frameworks^{18,19,21,23,27,38}). In this letter, we present two main extensions of the OC-CASSCF framework that enhance the method’s applicability. First, to go beyond the brute-force numerical orbital optimization of our previous work¹, we introduce a second-order Newton-Raphson scheme that incorporates the orthogonality constraints between multiple states. Second, motivated by the need to access response properties with practical applications (e.g. quantum dynamics, geometry optimizations), we propose a route to compute analytical nuclear gradients.

The letter is structured as follows. In Sec. I, we introduce the theoretical framework of OC-CASSCF. We then discuss practical two-step implementation and provide analytical expressions for the OC orbital Gradients and Hessians required in the Newton-Raphson optimization. An analytical form of the nuclear gradients is also presented for the OC-CASSCF energies. In Sec. II, we illustrate the performance of the method to describe the three lowest singlet states of the LiH molecule (and H₂O in Supplementary material 5). Finally, the use of the OC-CASSCF gradients is illustrated by performing geometry optimizations of the two molecular excited states.

I. THEORY

A. Orthogonally Constrained-CASSCF (OC-CASSCF)

Within the OC-CASSCF method, the goal is to approximate the low-lying eigenspectrum of a many-electron system (ground and excited states) *via* the optimization, at both orbital and CI levels, of a series of wavefunction ansätze $\{|\Psi_I(\kappa, \mathbf{c})\rangle\}$ while simultaneously enforcing their mutual orthogonality (*i.e.* $\langle\Psi_I(\kappa, \mathbf{c})|\Psi_{I'}(\kappa', \mathbf{c}')\rangle = \delta_{II'}$). To proceed, each state is described by a standard CASSCF-like ansatz

$$|\Psi_I(\kappa, \mathbf{c})\rangle = e^{-\hat{\kappa}} \sum_i c_i |\Phi_i^{\text{CAS}}\rangle, \quad (1)$$

with CI coefficients $\mathbf{c} = (\dots, c_i, \dots)$ (where $|\Phi_i^{\text{CAS}}\rangle$ are active-space Slater determinants or configuration state functions), and MO-rotation parameters $\kappa = (\dots, \kappa_{pq}, \dots)$ defining the generatrix $\hat{\kappa} = \sum_{p>q}^{\text{MOs}} \kappa_{pq} (\hat{E}_{pq} - \hat{E}_{qp})$ where $\hat{E}_{pq} = \sum_{\sigma \in \{\uparrow, \downarrow\}} \hat{a}_{p,\sigma}^\dagger \hat{a}_{q,\sigma}$ and $\hat{a}_{p,\sigma}^\dagger / \hat{a}_{p,\sigma}$ are spin-orbital creation/annihilation operators with spatial and spin parts p and σ respectively. To optimize these wavefunction ansätze and ensure mutual orthogonality between the OC-CASSCF states, one proceeds in an incremental way. First, the MOs and CI coefficients of a given wavefunction ansatz are optimized to describe a ground state. Then, to represent the first excited state, a new ansatz (with new CI and orbital parameters) is optimized now including an orthogonality constraint to enforce zero overlap with the previously optimized ground-state ansatz. This procedure is then systematically extended to higher-lying excited states, such that the K -th excited state is orthogonal to the K previously optimized states $\{|\Psi_I\rangle\}_{I=0}^{K-1}$. Importantly, at the end of this optimization protocol, each state is characterized by its own independent set of optimal MOs and CI coefficients.

From a formal point of view, optimizing a given K -th excited state with the OC-CASSCF scheme can be seen as a combined “CI+Orbital” optimization problem over the penalized energy functional $E_K^{\text{OC}}(\kappa, \mathbf{c})$ given by

$$\begin{aligned} \min_{\kappa, \mathbf{c}} E_K^{\text{OC}}(\kappa, \mathbf{c}) &= \min_{\kappa, \mathbf{c}} [\langle \Psi_K(\kappa, \mathbf{c}) | \hat{H}_K^{\text{OC}} | \Psi_K(\kappa, \mathbf{c}) \rangle] \\ &= \min_{\kappa, \mathbf{c}} [\langle \Psi_K(\kappa, \mathbf{c}) | (\hat{H} + \hat{P}_K^{\text{OC}}) | \Psi_K(\kappa, \mathbf{c}) \rangle] \quad (2) \\ &= \min_{\kappa, \mathbf{c}} [\langle \hat{H} \rangle_{\Psi_K} + \langle \hat{P}_K^{\text{OC}} \rangle_{\Psi_K}]. \end{aligned}$$

which satisfies orbital and CI stationarity conditions:

$$\frac{\partial E_K^{\text{OC}}}{\partial \kappa} = \mathbf{0}, \quad \frac{\partial E_K^{\text{OC}}}{\partial \mathbf{c}} = \mathbf{0}. \quad (3)$$

The penalized energy functional E_K^{OC} in Eq. (2) is expressed as the expectation value of an “Orthogonally Constrained (OC) Hamiltonian” noted \hat{H}_K^{OC} . The first contribution $\langle \hat{H} \rangle_{\Psi_K}$ is the conventional electronic energy given by the electronic structure Hamiltonian

$$\hat{H} = \sum_{pq} h_{pq} \hat{E}_{pq} + \frac{1}{2} \sum_{pqrs} g_{pqrs} \hat{e}_{pqrs} + \mathcal{E}_{\text{Nuc}}, \quad (4)$$

where h_{pq} and g_{pqrs} are the one- and two-electron integrals associated to their respective excitation operators \hat{E}_{pq} , and $\hat{e}_{pqrs} = \sum_{pqrs} \hat{E}_{pq} \hat{E}_{rs} - \delta_{qr} \hat{E}_{ps}$ and \mathcal{E}_{Nuc} is the nuclear repulsion energy.

The second contribution in Eq. (2), noted $\langle \hat{P}_K^{\text{OC}} \rangle_{\Psi_K}$, enforces orthogonality with respect to previously optimized states. It is defined through the projector

$$\hat{P}_K^{\text{OC}} = \sum_{I=0}^{K-1} \Delta_I |\Psi_I\rangle \langle \Psi_I| \quad (5)$$

where Δ_I are the so-called penalty shifts (positive amplitudes) associated to the previously optimized states $\{|\Psi_I\rangle\}_{I=0}^{K-1}$. Within this framework, any trial state exhibiting a non zero overlap with previously optimized states $\{|\Psi_I\rangle\}_{I=0}^{K-1}$ incurs an energetic penalty proportional to Δ_I , thereby enforcing orthogonality in its optimization.

Interestingly, following the procedure defined in Eq. (2) provides a natural extension of the variational principle to excited states. Within this framework, each newly optimized state is constrained to lie above the previously obtained ones in energy, as the imposed orthogonality conditions prevent collapse onto lower-lying solutions (see Refs^{18,19,21,23,27}).

B. Practical Implementation: Two-Step Approach

As in conventional CASSCF methods, a simultaneous optimization of both CI and orbital parameters is computationally demanding. To address this, we build upon our previous work¹ and adopt a practical “two-step” approach that enforces the orthogonality constraints at both the CI and orbital levels. Within this framework, the K -th electronic state is obtained by decoupling the optimization into two successive steps described below.

a. Orthogonally Constrained Configuration-Interaction: In a first step, the CI parameters \mathbf{c} of the state $|\Psi_K\rangle$ are evaluated by solving the following OC-CASCI eigenvalue equation (assuming fixed parameters $\kappa = \kappa^*$):

$$\hat{P}^{\text{AS}}(\kappa^*) \hat{H}_K^{\text{OC}} \hat{P}^{\text{AS}}(\kappa^*) |\Psi_K\rangle = E_K |\Psi_K\rangle, \quad (6)$$

where $\hat{P}^{\text{AS}}(\kappa^*)$ projects onto the active-space many-body basis built on the frozen orbitals κ^* . Despite the presence of the subscript “ K ”, note that Eq. (6) actually represents a ground-state eigenvalue problem: the penalty terms introduced in Eq. (5) ensure that the ground state of the projected OC Hamiltonian $\hat{P}^{\text{AS}}(\kappa^*) \hat{H}_K^{\text{OC}} \hat{P}^{\text{AS}}(\kappa^*)$ corresponds to the targeted K -th excited state $|\Psi_K\rangle$.

b. Orthogonally Constrained Orbital-Optimization: The second step consists in optimizing the orbital parameters κ with fixed CI coefficients \mathbf{c}^* , while still enforcing orthogonality constraints. In our previous work¹, this orbital optimization was carried out in a “brute-force” manner using numerical optimizers, which becomes impractical for larger-scale systems. Here, we introduce a more efficient and systematic strategy based on a second-order Newton-Raphson

algorithm³⁹ incorporating orthogonality constraints. Within this framework, the orbital update is given by

$$\boldsymbol{\kappa} \leftarrow \boldsymbol{\kappa} - (\mathbf{H}^{\text{OC}})^{-1} \mathbf{G}^{\text{OC}} \quad (7)$$

where we have introduced the OC orbital Gradient \mathbf{G}^{OC} and Hessian \mathbf{H}^{OC} including both an energy and an overlap part:

$$\begin{aligned} G_{pq}^{\text{OC}} &= G_{pq}^{\text{Energy}} + G_{pq}^{\text{Overlap}}, \\ H_{pq,rs}^{\text{OC}} &= H_{pq,rs}^{\text{Energy}} + H_{pq,rs}^{\text{Overlap}}. \end{aligned} \quad (8)$$

Analytical expressions for the energy contributions to the Gradient and Hessian are already well-known in the literature (see Refs^{28,39} for more details). Here, we present the analytical forms of the overlap contributions, which, to our knowledge, have never been introduced (see Supplementary Material 1 for a detailed derivation and possible simplifications):

$$G_{pq}^{\text{Overlap}} = 2 \sum_{I=0}^{K-1} \Delta_I S^{\Psi_K, \Psi_I} (\gamma_{pq}^{\Psi_K, \Psi_I} - \gamma_{qp}^{\Psi_K, \Psi_I}), \quad (9a)$$

$$\begin{aligned} H_{pq,rs}^{\text{Overlap}} &= 2 \sum_{I=0}^{K-1} \Delta_I (\gamma_{pq}^{\Psi_K, \Psi_I} - \gamma_{qp}^{\Psi_K, \Psi_I}) (\gamma_{rs}^{\Psi_K, \Psi_I} - \gamma_{sr}^{\Psi_K, \Psi_I}) \\ &+ \sum_{I=0}^{K-1} \Delta_I S^{\Psi_K, \Psi_I} \left(2(\Gamma_{pqrs}^{\Psi_K, \Psi_I} - \Gamma_{qprs}^{\Psi_K, \Psi_I} - \Gamma_{pqsr}^{\Psi_K, \Psi_I} + \Gamma_{qpsr}^{\Psi_K, \Psi_I}) \right. \\ &+ \delta_{rq}(\gamma_{ps}^{\Psi_K, \Psi_I} + \gamma_{sp}^{\Psi_K, \Psi_I}) - \delta_{sq}(\gamma_{pr}^{\Psi_K, \Psi_I} + \gamma_{rp}^{\Psi_K, \Psi_I}) \\ &\left. - \delta_{rp}(\gamma_{qs}^{\Psi_K, \Psi_I} + \gamma_{sq}^{\Psi_K, \Psi_I}) + \delta_{sp}(\gamma_{qr}^{\Psi_K, \Psi_I} + \gamma_{rq}^{\Psi_K, \Psi_I}) \right) \end{aligned} \quad (9b)$$

where $S^{\Psi_K, \Psi_I} = \langle \Psi_K | \Psi_I \rangle$, while $\gamma_{pq}^{\Psi_K, \Psi_I} = \langle \Psi_K | \hat{E}_{pq} | \Psi_I \rangle$ and $\Gamma_{pqrs}^{\Psi_K, \Psi_I} = \langle \Psi_K | \hat{e}_{pqrs} | \Psi_I \rangle$ represent one- and two-electron transition reduced density matrices (TRDMs) respectively. These quantities are discussed in Supplementary Material 2.

Implementing the OC Newton-Raphson step as defined in Eq. (7) provides a simultaneous “energy + overlap” optimization for the targeted state Ψ_K at the orbital level. At the end of this orbital optimization, the updated MOs are used to build a new CAS-CI problem to be solved, as given in Eq. (6). This alternating procedure between CI and orbital optimization is iterated self-consistently until convergence in the total energy.

Importantly, while we focus here on a two-step approach, an alternative “one-step” implementation of the OC-CASSCF method is also possible in principle. It would consist in a generalized Newton-Raphson optimization that simultaneously updates both the CI and orbital parameters³⁹. In addition to the orbital derivatives of Eq. (9), this scheme would require the OC Gradient and Hessian with respect to the CI coefficients, as well as the mixed CI-orbital Hessian. Although not the main focus of this work, analytical expressions of these quantities are provided in Supplementary Material 3 for the sake of completeness.

C. Analytical OC-CASSCF Nuclear Gradients

As a follow-up on OC-CASSCF electronic states and spectrum construction, we also introduce a strategy to compute the

nuclear gradients for both ground and excited states. From a practical perspective, these gradients are essential for applications such as geometry optimization and the computation of nuclear forces in *ab initio* quantum dynamics. Accessing an analytical form of such gradients is particularly important, as it offers significant advantages in numerical stability and computational efficiency compared to purely numerical finite-difference approaches.

To derive an analytical expression for the OC-CASSCF gradients, we build on the framework discussed in Refs.⁴⁰⁻⁴². More specifically, in fully variational state-specific electronic structure methods where both orbital and CI parameters are fully optimized (such as ground-state CASSCF or Hartree-Fock), the gradient of any individual electronic state can be substantially simplified. In particular, the total derivative of the energy E of a given state with respect to a nuclear coordinate x reads

$$\frac{dE}{dx} = \frac{\partial E}{\partial x} + \frac{\partial E}{\partial \mathbf{c}} \frac{\partial \mathbf{c}}{\partial x} + \frac{\partial E}{\partial \boldsymbol{\kappa}} \frac{\partial \boldsymbol{\kappa}}{\partial x}. \quad (10)$$

From the CI and Orbital stationarity conditions $\partial E / \partial \mathbf{c} = 0$ and $\partial E / \partial \boldsymbol{\kappa} = 0$ (fulfilled within such fully variational methods), the nuclear gradient reduces to the expectation value of the Hamiltonian derivative $\partial \hat{H} / \partial x$ (see Refs.^{28,40,41,43} and Supplementary Material 4)

$$\frac{dE}{dx} = \frac{\partial E}{\partial x} = \langle \Psi | \frac{\partial \hat{H}}{\partial x} | \Psi \rangle. \quad (11)$$

As shown in Eq. (3), the OC-CASSCF approach fulfills similar stationarity conditions on both CI and orbital parameters. Consequently, the OC-CASSCF analytical gradients are expected to retain the same form as in Eq. (11) for any optimized electronic state (ground and excited). In the following, we will show that this approach indeed yields consistent results compared to a numerical finite-difference approach.

II. NUMERICAL RESULTS

We now illustrate the performance of the OC-CASSCF method on the LiH molecule (see Supplementary Material 5 for similar inspections on the H₂O molecule). We focus on the three lowest singlet states and compare the results with FCI references, as well as with standard SA-CASSCF calculations. All results and method implementations are obtained using the open-source package *QuantNBody*⁴⁴, which enables a systematic representation of second-quantized operators and many-body wavefunctions. This package is used in conjunction with the quantum chemistry software *Psi*⁴⁵, which provides the required *ab initio* quantities. All calculations are performed using a minimal STO-6G basis set, without imposing any spatial symmetry.

A. Energies and Wavefunctions Properties

Energies and wavefunction properties for LiH are shown on Fig. 1 as a function of the internuclear distance x . FCI references account for the correlation of four electrons across six

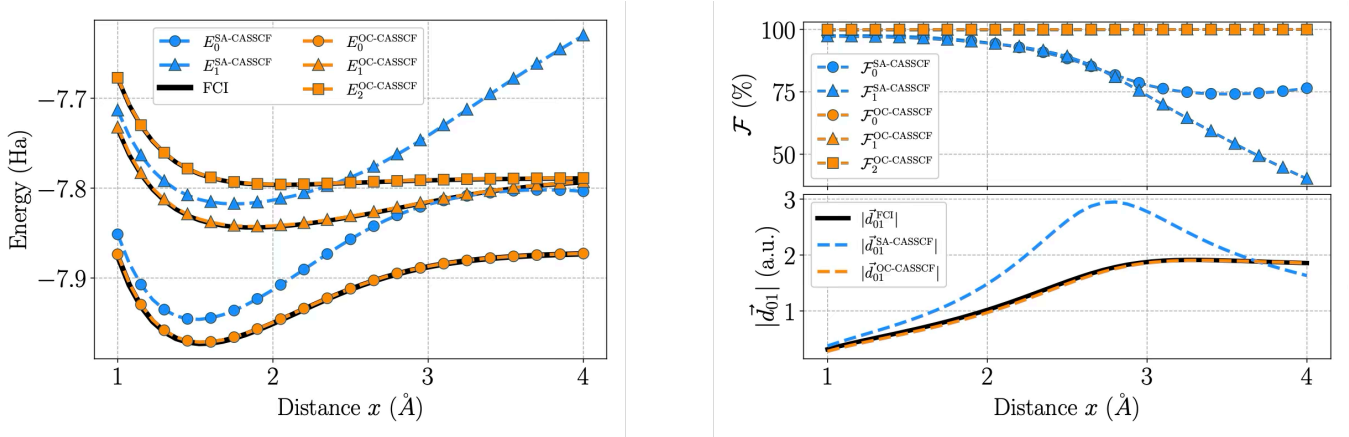


Figure 1: Evolution of energies and wavefunction-based properties for LiH (with a minimal STO-6G basis set and a penalty term $\Delta = 1$ Ha). Left panel: Dissociation curves for the three low-lying singlet states of the molecule. The solid black curves show the FCI reference results. The blue curves with markers represent the ground and first excited states obtained using the SA-CASSCF method. Similarly, the orange curves with markers correspond to the ground, first and second excited states obtained with the OC-CASSCF method. Right top panel: evolution of the state fidelity (as defined in Eq. (12)) of the SA-CASSCF and OC-CASSCF states relative to the FCI reference. Right bottom panel: evolution of the transition dipole magnitude between the ground and first excited states (as defined in Eq. (13)) obtained with SA-, OC-CASSCF and FCI.

orbitals, whereas both the OC-CASSCF and SA-CASSCF calculations were performed at the CAS(2,2) level. One should mention that OC-CASSCF calculations were run to describe all three low-lying states of the system (as in FCI), while SA-CASSCF were restricted to the ground and first excited states.

In the left panel of Fig. 1, the dissociation curves obtained with OC-CASSCF are shown as orange dashed lines, SA-CASSCF as blue dashed lines, and FCI references as solid black lines. As readily seen, the three low-lying OC-CASSCF energies closely match the FCI references across the entire range of internuclear distances. Additional numerical inspections (not shown in Fig. 1) indicate here a maximum energy error of $\sim 2 \times 10^{-3}$ Ha with respect to FCI. In contrast, the SA-CASSCF energies deteriorate rapidly as the distance increases, exhibiting a much stronger ~ 0.16 Ha deviation.

Even with a minimal CAS(2,2) active space, these results reveal that OC-CASSCF provides a more accurate description of the three low-lying energies as compared to SA-CASSCF, which optimizes only two states (same observations as in Refs. ^{36,37}).

To be reliable, a method should not only provide accurate energies but also proper electronic wavefunctions and related properties. Therefore, we considered two complementary wavefunction-based measures. The first one is the state-specific fidelity with respect to the FCI wavefunctions,

$$\mathcal{F}_K^{\text{Method}} = |\langle \Psi_K^{\text{FCI}} | \Psi_K^{\text{Method}} \rangle|^2. \quad (12)$$

Following this definition, the closer $\mathcal{F}_K^{\text{Method}}$ is to 100%, the closer the wavefunction obtained with a given CAS "Method" (here, either OC- or SA-CASSCF) is to the exact FCI state.

In the top-right panel of Fig. 1, we report the evolution of the OC- and SA-CASSCF state fidelities as a function of the internuclear distance x . The OC-CASSCF results (orange curves) for the three electronic states remain very close

to unity over the entire range of x distance values. A more detailed analysis (not shown) reveals that the $\mathcal{F}_{\text{OC-CASSCF}}$ fidelity consistently exceeds 99.7% for all three states. In contrast, the fidelities obtained with SA-CASSCF deteriorate markedly as the internuclear distance x increases. In particular, the lowest fidelities can be as low as 70% and 40% for the ground and first excited states, respectively.

As a second measure of the wavefunction quality, we consider a physically motivated observable: the transition dipole moment. The latter provides direct insight into the electronic redistribution upon photo-excitation and plays a central role in optical transition probabilities and spectroscopic intensities. More specifically, we evaluate the magnitude of the transition dipole between the ground and first excited states

$$|\vec{d}_{01}^{\text{Method}}| = \sqrt{\sum_{\alpha=X,Y,Z} |\langle \Psi_0^{\text{Method}} | \hat{d}^{(\alpha)} | \Psi_1^{\text{Method}} \rangle|^2}, \quad (13)$$

where $\hat{d}^{(\alpha)}$ is the dipole operator along the α direction

$$\hat{d}^{(\alpha)} = \sum_{pq} \left(d_{pq}^{\text{elec}(\alpha)} + d_{pq}^{\text{nuc}(\alpha)} \delta_{pq} \right) \hat{E}_{pq}, \quad (14)$$

where $d_{pq}^{\text{elec}(\alpha)}$ and $d_{pq}^{\text{nuc}(\alpha)}$ are the electronic dipole integrals and the scalar nuclear dipole, respectively. Note in Eq. (13) that the superscript "Method" will cover the three approaches FCI, OC- and SA-CASSCF. The resulting dipole magnitudes are shown in the bottom-right panel of Fig. 1 as a function of the internuclear distance x . The exact FCI reference (black curve) exhibits two distinct behaviors: a nearly monotonic increase for $x \in [1\text{\AA}, 3\text{\AA}]$, followed by a *ca.* 2 a.u. plateau. The OC-CASSCF results (orange curve) closely reproduce this trend, providing further evidence of the high quality of the ground and first excited wavefunctions. A more detailed numerical analysis (not shown here) indicates that the maximum

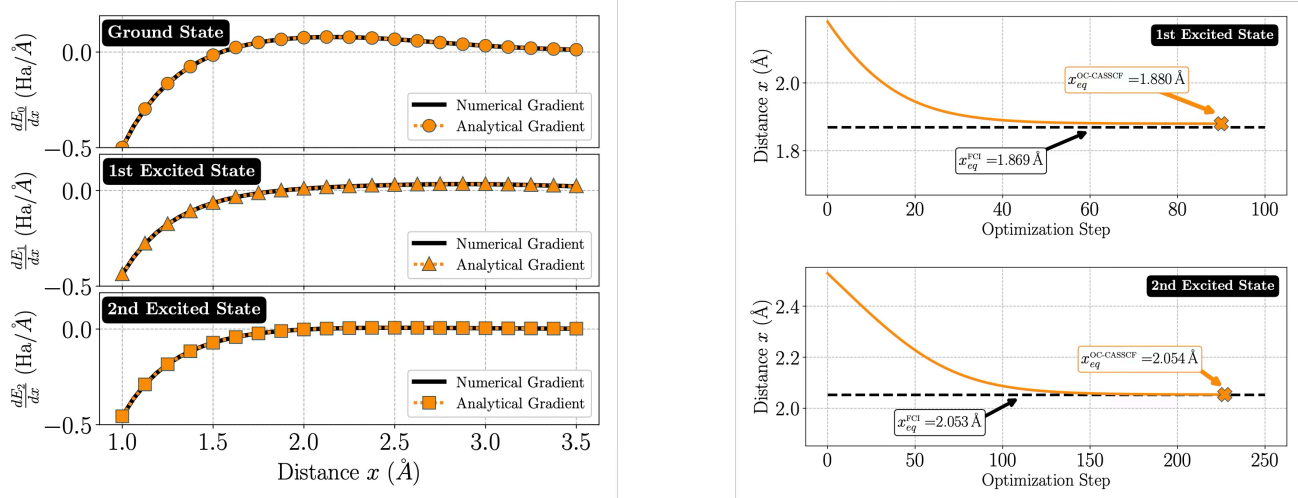


Figure 2: Illustration of the nuclear gradients computation for the LiH molecule (using minimal STO-6G basis set with $\Delta = 1$ Ha). Left panels: Gradient amplitudes across the internuclear distance for the ground, first and second excited states. Analytical gradients are shown with orange curves, while black full lines are used for numerical gradients. Right panels: Geometry optimization for the two excited states using a gradient descent approach with $\eta = 1$ (see Eq. (15)). Evolution of internuclear distance x at each optimization step (orange full line). FCI equilibrium positions are shown with black dashed lines.

deviation from the FCI reference remains below 5×10^{-2} a.u. over the entire range of internuclear distances. In contrast, the SA-CASSCF method significantly overestimates the transition dipole and additional numerical analysis indicate a maximum deviation of 1.6 a.u. compared to FCI results.

Overall, these observations, together with the state fidelity and the energy comparisons with respect to FCI, demonstrate that OC-CASSCF provides a more consistent description of both electronic energies and wavefunction-related properties than SA-CASSCF. Taken together, these results provide clear evidence that the use of a shared set of optimized orbitals within a state-averaged approach can sometimes significantly compromise the quality of both energies and wavefunctions. Note that similar observations were also obtained for the H₂O molecule, as reported in Supplementary Material 5.

B. Nuclear Gradients and Geometry Optimizations

To conclude on the LiH system, we discuss the evaluation of nuclear gradients within the OC-CASSCF framework and illustrate their use in a practical geometry optimization. We first examine the three left panels of Fig. 2, which show the evolution of gradient amplitudes for the ground, first and second excited states as a function of the internuclear distance x . Here, analytical gradient amplitudes computed from Eq. (11) (orange curves) are compared with numerical gradients (black curves) obtained via a two-point finite-difference scheme. For all three states, excellent agreement is observed between the analytical and numerical approaches, with a negligible discrepancy of at most 10^{-4} Ha/Å across the full range of internuclear distances x .

As a practical application, we employed the analytical gradients to perform geometry optimizations of the two sin-

glet excited states of LiH. As previously shown in Fig. 1, the FCI dissociation curves for the first and second excited states each display a single energy minimum, with equilibrium distances of $x_{eq}^{FCI} = 1.87$ Å and 2.05 Å, respectively. To compare, the equilibrium distances $x_{eq}^{OC-CASSCF}$ that define the OC-CASSCF dissociation curves minima were located via a gradient-descent procedure:

$$x^{n+1} = x^n - \eta \left. \frac{dE_K}{dx} \right|_{x=x^n}, \quad (15)$$

where η is a fixed damping parameter, x^n is the geometry at step n , and $\frac{dE_K}{dx}$ is evaluated based on Eq. (11). The top-right and bottom-right panels of Fig. 2 show the optimization trajectories for the first and second excited states, respectively (see caption for simulation details). Interestingly, for both states, the optimized OC-CASSCF geometries are very close to the FCI equilibrium points, with $|x_{eq}^{OC-CASSCF} - x_{eq}^{FCI}| < 10^{-2}$ Å.

These results further underscore the high quality of the dissociation curves produced by OC-CASSCF compared to FCI, and also confirm the accuracy and reliability of the analytical gradient in practical geometry optimizations for locating the associated spectral features. Note again that similar observations were also obtained for the H₂O molecule, as reported in Supplementary Material 5.

CONCLUSION

In this work, we have presented several theoretical extensions to the previously introduced orthogonally constrained version of the CASSCF method (OC-CASSCF)¹. We introduced a two-step procedure based on a second-order Newton-Raphson scheme for orthogonally constrained orbital opti-

mization, for which analytical expressions of the constrained orbital Gradients and Hessians have been derived. As a possible extension toward a direct one-step formulation, complementary Gradients and Hessians for the CI and orbital-CI blocks are also provided (see Supplementary Material 3). In addition, we have discussed a route to compute analytical nuclear gradients, enabling the application of OC-CASSCF to geometry optimizations and related studies. Based on these tools, the performance of the OC-CASSCF procedure was assessed by optimizing the three lowest singlet states of LiH (and H₂O in Supplementary material 5). The resulting energies and states show very good agreement with reference Full CI results, whereas SA-CASSCF fails to provide an adequate description. Analytical nuclear gradients were further employed in geometry optimizations to accurately locate the local minima of the first and second excited states.

Naturally, this work should be regarded as preliminary, focusing on the prototyping of OC-CASSCF for small molecules using minimal basis sets. The very good agreement observed with FCI results is encouraging, but should not be considered definitive or systematic. Larger-scale simulations of more complex systems will be required in future, and we hope that the tools and demonstrations presented here will facilitate future implementations of OC-CASSCF in advanced electronic-structure packages. For larger and more practical systems, CAS calculations will naturally require subsequent perturbative treatments (e.g., CASPT2 or NEVPT2^{46–49}) to approach FCI accuracy. In this broader context, it remains to be explored whether OC-CASSCF can provide a more reliable zeroth-order description than the standard state-averaged approach for such perturbative corrections. These questions are left for future work.

SUPPLEMENTARY MATERIAL

- Derivation of the analytical expressions for the overlap orbital Gradient and Hessian.
- Analytical expressions for the TRDMs when one of the states belongs to the CAS.
- Derivation of analytical expressions for the overlap configuration Gradient and Hessian and for the overlap mixed Hessian in the case of a one-step optimization.
- Analytical expression of the derivative of the Hamiltonian operator.
- Numerical results for the first and second excited states of the H₂O molecule (potential energy surfaces, transition dipole moments and geometry optimization).

ACKNOWLEDGMENTS

This work benefited from State support managed by the ANR under the France 2030 program, referenced by ANR-23-PETQ-0006. It is also supported by the Interdisciplinary Thematic Institute QMat, as part of the ITI 2021-2028 program of

the University of Strasbourg, CNRS and Inserm, and was supported by IdEx Unistra (ANR-10-IDEX-0002), SFRI STRAT' US project (ANR-20-SFRI-0012), and EUR QMAT (ANR-17-EURE-0024). Both these fundings were granted under the framework of the French Investments for the Future Program.

REFERENCES

- S. Yalouz and V. Robert, *Journal of chemical theory and computation* **19**, 1381 (2023).
- S. Bonnet, *Journal of the American Chemical Society* **145**, 23397 (2023).
- M. B. Smith and J. Michl, *Annual review of physical chemistry* **64**, 361 (2013).
- P. Roseiro, A. Shah, S. Yalouz, and V. Robert, *ChemPhysChem* **26**, e202400914 (2025).
- P. Roseiro, S. Yalouz, D. J. Brook, N. Ben Amor, and V. Robert, *Inorganic Chemistry* **62**, 5737 (2023).
- D. Sheng, Z. Weng, C. Ting, and J. Dong, *Physical Review B* **49**, 4279 (1994).
- M. Vérot, S. A. Borshch, and V. Robert, *Chemical Physics Letters* **519**, 125 (2012).
- S. Vela, M. Verot, E. Fromager, and V. Robert, *The Journal of Chemical Physics* **146** (2017).
- R. A. Marcus, *Angewandte Chemie International Edition in English* **32**, 1111 (1993).
- A. Domingo, C. Angeli, C. de Graaf, and V. Robert, *Journal of Computational Chemistry* **36**, 861 (2015).
- W. Hunt, T. Dunning Jr, and W. Goddard III, *Chemical Physics Letters* **3**, 606 (1969).
- A. T. Gilbert, N. A. Besley, and P. M. Gill, *The Journal of Physical Chemistry A* **112**, 13164 (2008).
- G. M. Barca, A. T. Gilbert, and P. M. Gill, *Journal of chemical theory and computation* **14**, 1501 (2018).
- A. J. Thom and M. Head-Gordon, *Physical review letters* **101**, 193001 (2008).
- M. Dash, J. Feldt, S. Moroni, A. Scemama, and C. Filippi, *Journal of chemical theory and computation* **15**, 4896 (2019).
- M. Dash, S. Moroni, C. Filippi, and A. Scemama, *Journal of chemical theory and computation* **17**, 3426 (2021).
- A. Cuzzocrea, S. Moroni, A. Scemama, and C. Filippi, *Journal of chemical theory and computation* **18**, 1089 (2022).
- S. Shepard, R. L. Panades-Barrueta, S. Moroni, A. Scemama, and C. Filippi, *Journal of chemical theory and computation* **18**, 6722 (2022).
- S. Pathak, B. Busemeyer, J. N. Rodrigues, and L. K. Wagner, *The Journal of Chemical Physics* **154** (2021).
- S. R. White, *Physical review b* **48**, 10345 (1993).
- E. M. Stoudenmire and S. R. White, *Annu. Rev. Condens. Matter Phys.* **3**, 111 (2012).
- G. K. Chan, A. Keselman, N. Nakatani, Z. Li, and S. R. White, *The Journal of chemical physics* **145** (2016).
- M. Fishman, S. White, and E. M. Stoudenmire, *SciPost Physics Codebases* , 004 (2022).
- A. Marie, F. Kossoski, and P.-F. Loos, *The Journal of Chemical Physics* **155** (2021).
- F. Kossoski, A. Marie, A. Scemama, M. Caffarel, and P.-F. Loos, *Journal of Chemical Theory and Computation* **17**, 4756 (2021).
- Y. Damour, A. Scemama, D. Jacquemin, F. Kossoski, and P.-F. Loos, *Journal of Chemical Theory and Computation* **20**, 4129 (2024).
- G. Zhu, J. Bierman, J. Lu, and Y. Li, “State-specific orbital optimization for enhanced excited-states calculation on quantum computers,” (2025), arXiv:2510.13544 [quant-ph].
- S. Yalouz, E. Koridon, B. Senjean, B. Lasorne, F. Buda, and L. Visscher, *Journal of chemical theory and computation* **18**, 776 (2022).
- S. Yalouz, B. Senjean, J. Günther, F. Buda, T. E. O'Brien, and L. Visscher, *Quantum Sci. Technol.* **6**, 024004 (2021).
- O. Higgott, D. Wang, and S. Brierley, *Quantum* **3**, 156 (2019).

³¹K. M. Nakanishi, K. Mitarai, and K. Fujii, *Phys. Rev. Res.* **1**, 033062 (2019).

³²P. E. Siegbahn, J. Almlöf, A. Heiberg, and B. O. Roos, *J. Chem. Phys.* **74**, 2384 (1981).

³³P. Å. Malmqvist, B. O. Roos, and B. Schimmelpfennig, *Chem. Phys. Lett.* **357**, 230 (2002).

³⁴W. Dobroutz, O. Weser, N. A. Bogdanov, A. Alavi, and G. Li Manni, *Journal of Chemical Theory and Computation* **17**, 5684 (2021).

³⁵G. L. Manni, I. F. Galván, A. Alavi, F. Aleotti, F. Aquilante, J. Autschbach, D. Avagliano, A. Baiardi, J. J. Bao, S. Battaglia, *et al.*, *Journal of chemical theory and computation* **19**, 6933 (2023).

³⁶A. Marie and H. G. Burton, *The Journal of Physical Chemistry A* **127**, 4538 (2023).

³⁷S. Saade and H. G. Burton, *Journal of Chemical Theory and Computation* **20**, 5105 (2024).

³⁸G. Levi, A. V. Ivanov, and H. Jónsson, *Faraday Discussions* **224**, 448 (2020).

³⁹T. Helgaker, P. Jorgensen, and J. Olsen, *Molecular electronic-structure theory* (John Wiley & Sons, 2014).

⁴⁰T. U. Helgaker and J. Almlöf, *Int. J. Quantum Chem.* **26**, 275 (1984).

⁴¹T. Helgaker, N. Allinger, T. Clark, J. Gasteiger, P. Kollmann, H. SchaeferIII, P. Schreiner, *et al.*, “Gradient theory,” (1998).

⁴²Y. Yamaguchi and H. F. Schaefer III, *Handbook of High-resolution Spectroscopy* (2011).

⁴³J. Ståring, A. Bernhardsson, and R. Lindh, *Mol. Phys.* **99**, 103 (2001).

⁴⁴S. Yalouz, M. R. Gullin, and S. Sekaran, *Journal of Open Source Software* **7**, 4759 (2022).

⁴⁵D. G. Smith, L. A. Burns, A. C. Simonett, R. M. Parrish, M. C. Schieber, R. Galvelis, P. Kraus, H. Kruse, R. Di Remigio, A. Alenaizan, *et al.*, *J. Chem. Phys.* **152**, 184108 (2020).

⁴⁶B. O. Roos, P. Linse, P. E. Siegbahn, and M. R. Blomberg, *Chemical Physics* **66**, 197 (1982).

⁴⁷K. Andersson, P.-Å. Malmqvist, and B. O. Roos, *J. Chem. Phys.* **96**, 1218 (1992).

⁴⁸C. Angeli, R. Cimiraglia, S. Evangelisti, T. Leininger, and J.-P. Malrieu, *J. Chem. Phys.* **114**, 10252 (2001).

⁴⁹C. Angeli, S. Borini, M. Cestari, and R. Cimiraglia, *J. Chem. Phys.* **121**, 4043 (2004).